

# Bound-state band reconstruction and resonance in a spin-1/2 Bose gas with one-dimensional spin-orbit coupling

Qi Gu, Yuncheng Xiong, and Lan Yin\*

*School of Physics, Peking University, Beijing 100871, China*

 (Received 12 December 2019; accepted 28 January 2020; published 18 February 2020)

In this paper, we study two-body bound states in two-component Bose gas with a one-dimensional spin-orbit coupling induced by Raman lasers. The finite Raman coupling strength generates coupling among three spin channels, resulting in the reconstruction of three bound-state bands. In addition, multiple resonances can be induced at finite scattering lengths. By tuning the interaction in one intraspecies channel, one bound-state band can be lifted and three resonances can be achieved, which can be observable under current experimental conditions in  $^{87}\text{Rb}$  atoms. This induced resonance is helpful for imaging the density modulation in the stripe phase.

DOI: [10.1103/PhysRevA.101.023609](https://doi.org/10.1103/PhysRevA.101.023609)

## I. INTRODUCTION

Synthetic spin-orbit coupling (SOC) is an important tool in the study ultracold quantum gases. There have been a lot of experimental and theoretical studies on spin-orbit coupled quantum gases during the past decade [1–4]. One-dimensional (1D) SOC was first generated by dressing two hyperfine spin states with a pair of lasers in a  $^{87}\text{Rb}$  Bose-Einstein condensate [5]. A similar scheme was also used to generate 1D SOC in  $^{40}\text{K}$  [6] and  $^6\text{Li}$  [7] Fermi gases. Two-dimensional SOC has been experimentally realized in  $^{40}\text{K}$  gases with three Raman lasers [8] and in  $^{87}\text{Rb}$  atoms with an optical Raman lattice [9]. Bose gases with 1D SOC can condense into the stripe phase, magnetized phase, or nonmagnetized phase for different SOC parameters [5,10,11]. The stripe phase breaks the translational and  $U(1)$  symmetries simultaneously, consistent with the definition of the supersolid phase. Although it has been observed experimentally [5,10,12–15], the density modulation has not been directly imaged so far. Fermi gases with SOC were predicted to be unconventional superfluid at low temperatures [16–18]. Condensation of two-body bound states was predicted not only in Fermi gases [19,20], but also in Bose gases with SOC [21,22].

How SOC affects bound-state formation and atom scattering generally in a Bose gas with SOC is an important and unanswered problem. Interactions between atoms can be strongly altered by the light dressed as in Refs. [23,24]. Previous studies showed that, in the case of fermions with 1D SOC, finite Raman strength can shift the location of the Feshbach resonance [24–27]. In a Bose gas with anisotropic SOC, one can induce resonance by tuning the anisotropy of SOC strengths [28]. In the case with Rashba SOC, the resonance position can only be shifted in intraspecies channels [21]. In the case with Weyl SOC, resonance positions of all three scattering channels are shifted [22]. Nonetheless, in the

case of 1D SOC with vanishing Raman coupling, the SOC does not change either the resonance position or bound-state binding energy.

In this paper, we study two-body bound states in spin-1/2 Bose gas with 1D SOC at finite Raman coupling. The Raman coupling can be viewed as the effective Zeeman field that causes spin-flipping processes. We find that three scattering channels are coupled together, resulting in the formation of three new bound-state bands. The finite Raman coupling also induces resonances at finite scattering lengths. By tuning the scattering length in one intraspecies channel, one bound-state band can be lifted up and the resonance locations can be shifted. We propose a scheme to observe this resonance in the  $^{87}\text{Rb}$  system, which can be helpful to directly image the periodic structure in the stripe phase.

## II. ENERGY BANDS OF TWO-BODY BOUND STATES IN THE PRESENCE OF 1D SOC

### A. Model

We consider a two-component homogeneous Bose gas with a Raman-induced SOC, described by the Hamiltonian  $H = H_0 + H_{\text{int}}$ . The single-particle term is given by

$$H_0 = \sum_{\mathbf{k}\rho\rho'} \left[ \epsilon_k \delta_{\rho\rho'} + \frac{\Omega}{2} \sigma_{x\rho\rho'} + \left( \frac{\hbar^2 k_0}{m} k_x + \frac{\delta_z}{2} \right) \sigma_{z\rho\rho'} \right] c_{\mathbf{k}\rho}^\dagger c_{\mathbf{k}\rho'}, \quad (1)$$

where  $c_{\mathbf{k}\rho}^\dagger$  is the creation operator of a boson with momentum  $\hbar\mathbf{k}$  and spin component  $\rho = \uparrow$  or  $\downarrow$ ,  $\Omega$  is the Raman coupling strength,  $k_0$  is the SOC strength, and  $\delta_z$  is the detuning energy,  $\sigma_x$  and  $\sigma_z$  are Pauli matrices, and  $\epsilon_k = \hbar^2 k^2 / (2m)$ . The recoil energy is defined as  $E_r = \hbar^2 k_0^2 / (2m)$ . The single-particle Hamiltonian  $H_0$  can be diagonalized, yielding two helical excitation branches  $\epsilon_{\mathbf{k}}^\pm = \epsilon_{\mathbf{k}} \pm \sqrt{\Omega^2/4 + (\hbar^2 k_0 k_x / m + \delta_z/2)^2}$ . Note that the single-particle Hamiltonian  $H_0$  is written in the moving frame of reference where the momentum  $\hbar\mathbf{k}$

\*yinlan@pku.edu.cn

corresponds to the momentum  $\hbar(\mathbf{k} - \mathbf{k}_0)$  for spin-up atoms or  $\hbar(\mathbf{k} + \mathbf{k}_0)$  for spin-down atoms in the laboratory frame. For simplicity, we just consider the case with zero detuning  $\delta_z = 0$ . The energy minimum of the lower branch  $\epsilon_{\mathbf{k}}^-$  is given by

$$E_{\min} = \begin{cases} \epsilon_{\pm\mathbf{q}_0}^- = -E_r - \Omega^2/(16E_r), & \Omega < 4E_r \\ \epsilon_0^- = -\Omega/2, & \Omega > 4E_r \end{cases}, \quad (2)$$

where  $\mathbf{q}_0 = \mathbf{k}_0\sqrt{1 - \Omega^2/(4E_r)^2}$  and  $\mathbf{k}_0 = k_0\hat{x}$ . The spin-dependent  $s$ -wave interactions between bosons are given by

$$H_{\text{int}} = \frac{1}{2V} \sum_{\mathbf{k}\mathbf{k}'\mathbf{q}\rho\rho'} g_{\rho\rho'} c_{\mathbf{q}+\mathbf{k}'\rho}^\dagger c_{\mathbf{q}-\mathbf{k}'\rho'}^\dagger c_{\mathbf{q}-\mathbf{k}\rho'} c_{\mathbf{q}+\mathbf{k}\rho}, \quad (3)$$

where the  $s$ -wave coupling constant  $g_{\rho\rho'}$  is related to the scattering length in the absence of SOC  $a_{\rho\rho'}$  by the renormalization relation  $1/g_{\rho\rho'} = 1/g_{\rho\rho'} = m(4\pi\hbar^2 a_{\rho\rho'})^{-1} - \Lambda$  with  $\Lambda = \int d^3k (2\pi)^{-3} (2\epsilon_k)^{-1}$ .

### B. Two-body bound state

The eigenequation of a two-body bound state is given by  $H|\varphi\rangle = E_{2\mathbf{q}}|\varphi\rangle$ , where  $E_{2\mathbf{q}}$  and  $|\varphi\rangle = \frac{1}{2} \sum_{\mathbf{k}\rho\rho'} \phi_{\rho\rho'}(\mathbf{q}, \mathbf{k}) c_{\mathbf{q}+\mathbf{k}\rho}^\dagger c_{\mathbf{q}-\mathbf{k}\rho'}^\dagger |0\rangle$  are the bound-state eigenenergy and eigenstate with center-of-mass momentum (COMM)  $2\mathbf{q}$ . From the eigenequation, we obtain a set of linear equations for the coefficient  $\phi_{\rho\rho'}(\mathbf{q}, \mathbf{k})$ :

$$M_{\mathbf{k}\mathbf{q}} \Phi_{\mathbf{k}\mathbf{q}} = \mathbf{G} \frac{1}{V} \sum_{\mathbf{p}} \Phi_{\mathbf{p}\mathbf{q}}, \quad (4)$$

where  $\Phi_{\mathbf{k}\mathbf{q}} = [\phi_{\uparrow\uparrow}(\mathbf{q}, \mathbf{k}), \phi_{\downarrow\downarrow}(\mathbf{q}, \mathbf{k}), \phi_{\uparrow\downarrow}(\mathbf{q}, \mathbf{k}), \phi_{\downarrow\uparrow}(\mathbf{q}, \mathbf{k})]^T$ , and the matrix  $M_{\mathbf{k}\mathbf{q}}$  is given by

$$\begin{pmatrix} \xi_{\mathbf{k}\mathbf{q}} - \delta_z - 2h_{qx} & 0 & -\Omega/2 & -\Omega/2 \\ 0 & \xi_{\mathbf{k}\mathbf{q}} + \delta_z + 2h_{qx} & -\Omega/2 & -\Omega/2 \\ -\Omega/2 & -\Omega/2 & \xi_{\mathbf{k}\mathbf{q}} - 2h_{kx} & 0 \\ -\Omega/2 & -\Omega/2 & 0 & \xi_{\mathbf{k}\mathbf{q}} + 2h_{kx} \end{pmatrix}$$

with  $\xi_{\mathbf{k}\mathbf{q}} = E_{2\mathbf{q}} - \epsilon_{\mathbf{k}+\mathbf{q}} - \epsilon_{\mathbf{k}-\mathbf{q}}$ ,  $h_{kx} = \hbar^2 k_0 k_x / m$ , and the coupling matrix  $\mathbf{G}$  is given by  $G_{ij} = (g_{\uparrow\uparrow}\delta_{i1} + g_{\downarrow\downarrow}\delta_{i2} + g_{\uparrow\downarrow}\delta_{i3} + g_{\downarrow\uparrow}\delta_{i4})\delta_{ij}$ . Equation (4) can be further written as

$$\Gamma = \mathbf{G} \frac{1}{V} \sum_{\mathbf{k}} M_{\mathbf{k}\mathbf{q}}^{-1} \Gamma, \quad (5)$$

where  $\Gamma = \mathbf{G} \frac{1}{V} \sum_{\mathbf{p}} \Phi_{\mathbf{p}\mathbf{q}}$ . The eigenenergy  $E_{2\mathbf{q}}$  can be determined from the secular equation

$$\det \left( \mathbf{G} \frac{1}{V} \sum_{\mathbf{k}} M_{\mathbf{k}\mathbf{q}}^{-1} - \mathbf{I} \right) = 0. \quad (6)$$

Eigenenergies of both two-boson and two-fermion bound states satisfy Eq. (6). For two-boson bound state, Eq. (6) can be further written as

$$\det \begin{pmatrix} A_1 - 1/a_{\uparrow\uparrow} & \sqrt{2}C_1 & C_3 \\ \sqrt{2}C_1 & A_3 - 1/a_{\downarrow\downarrow} & \sqrt{2}C_2 \\ C_3 & \sqrt{2}C_2 & A_2 - 1/a_{\downarrow\downarrow} \end{pmatrix} = 0, \quad (7)$$

where  $A_{1,2,3}$  and  $C_{1,2,3}$  are functions of energy  $E_{2\mathbf{q}}$ , momentum  $2\hbar\mathbf{q}$ , and  $\Omega$ , as given below:

$$\begin{aligned} \frac{mA_{1,2}}{4\pi\hbar^2} &= \frac{1}{V} \sum_{\mathbf{k}} \frac{(\xi_{\mathbf{k}\mathbf{q}} \pm 2h_{qx})(\xi_{\mathbf{k}\mathbf{q}}^2 - 4h_{kx}^2) - \xi_{\mathbf{k}\mathbf{q}}\Omega^2/2}{(\xi_{\mathbf{k}\mathbf{q}}^2 - 4h_{qx}^2)(\xi_{\mathbf{k}\mathbf{q}}^2 - 4h_{kx}^2) - \xi_{\mathbf{k}\mathbf{q}}^2\Omega^2} + \Lambda, \\ \frac{mA_3}{4\pi\hbar^2} &= \frac{1}{V} \sum_{\mathbf{k}} \frac{\xi_{\mathbf{k}\mathbf{q}}(\xi_{\mathbf{k}\mathbf{q}}^2 - 4h_{qx}^2)}{(\xi_{\mathbf{k}\mathbf{q}}^2 - 4h_{qx}^2)(\xi_{\mathbf{k}\mathbf{q}}^2 - 4h_{kx}^2) - \xi_{\mathbf{k}\mathbf{q}}^2\Omega^2} + \Lambda, \\ \frac{mC_{1,2}}{4\pi\hbar^2} &= \frac{1}{V} \sum_{\mathbf{k}} \frac{\xi_{\mathbf{k}\mathbf{q}}(\xi_{\mathbf{k}\mathbf{q}} \pm 2h_{qx})\Omega/2}{(\xi_{\mathbf{k}\mathbf{q}}^2 - 4h_{qx}^2)(\xi_{\mathbf{k}\mathbf{q}}^2 - 4h_{kx}^2) - \xi_{\mathbf{k}\mathbf{q}}^2\Omega^2}, \\ \frac{mC_3}{4\pi\hbar^2} &= \frac{1}{V} \sum_{\mathbf{k}} \frac{\xi_{\mathbf{k}\mathbf{q}}\Omega^2/2}{(\xi_{\mathbf{k}\mathbf{q}}^2 - 4h_{qx}^2)(\xi_{\mathbf{k}\mathbf{q}}^2 - 4h_{kx}^2) - \xi_{\mathbf{k}\mathbf{q}}^2\Omega^2}. \end{aligned} \quad (8)$$

When the Raman strength  $\Omega$  is finite, all the off-diagonal matrix elements in Eq. (7) are finite, indicating that in the presence of Raman field the three spin channels  $\uparrow\uparrow$ ,  $\downarrow\downarrow$ , and  $\uparrow\downarrow$  mix together.

### C. Energy bands

In the zero Raman strength limit,  $C_{1,2,3} = 0$ , Eq. (7) is reduced to three independent equations. Three spin channels are decoupled, and the bound-state energy depends only on the scattering length of its spin channel, in the intraspecies channel

$$\frac{E_{2\mathbf{q}}}{2E_r} = \frac{E_{\min}}{E_r} - \frac{1}{k_0^2 a_{\rho\rho}^2} + \left(1 \pm \frac{q_x}{2k_0}\right)^2 + \left(\frac{q_{yz}}{2k_0}\right)^2 \quad (9)$$

and in the interspecies channel

$$\frac{E_{2\mathbf{q}}}{2E_r} = \frac{E_{\min}}{E_r} - \frac{1}{k_0^2 a_{\uparrow\downarrow}^2} + \left(\frac{q}{2k_0}\right)^2. \quad (10)$$

As shown in Fig. 1, the minimum of the bound-state band in the intraspecies  $\uparrow\uparrow$  ( $\downarrow\downarrow$ ) channel is located at COMM  $-2\hbar\mathbf{k}_0$  ( $+2\hbar\mathbf{k}_0$ ), while that in the interspecies  $\uparrow\downarrow$  channel is located at zero COMM. Bound states composed of two spin-1/2 atoms behave as a single spin-1 particle with a pure 1D SOC,  $\frac{\hbar^2 k_0 k_x}{m} F_z$ , where  $F_z$  is the  $z$ -component spin operator for the spin-1 bound state.

When Raman coupling strength is finite, the three parabolic bands are reconstructed to three new disjoint energy bands. As shown in Fig. 1(a), with symmetric interactions  $a_{\uparrow\uparrow} = a_{\downarrow\downarrow} = a_{\uparrow\downarrow} = a$ , the lowest band has three minimum points located near  $\pm 2\mathbf{k}_0$  and zero when  $\Omega$  is very small. In such case, to the first order of  $\Omega$ , bound states can be approximated as a spin-1 single particle with SOC described in Ref. [29]. As  $\Omega$  increases, two minimum points in the lowest band disappear and only the one at zero is left, as shown in Fig. 1(b). When  $\Omega > 4E_r$ , two minimum points in the middle band merge into one, as shown in Fig. 1(c). When the scattering length  $a$  increases, the bound states have less binding energy and all the bands are lifted up, as shown in Fig. 1(d).

The bound-state bands also change with the asymmetry of interactions. In an extreme case with  $a_{\downarrow\downarrow} = a_{\uparrow\downarrow} \ll a_{\uparrow\uparrow}$ , one band is lifted up with the band minimum located near COMM  $-2\hbar\mathbf{k}_0$ , as shown in Fig. 2(a). In another case with  $a_{\uparrow\uparrow} = a_{\downarrow\downarrow} \ll a_{\uparrow\downarrow}$ , one band is raised up with the band minimum located at zero COMM, as shown in Fig. 2(b). In these two

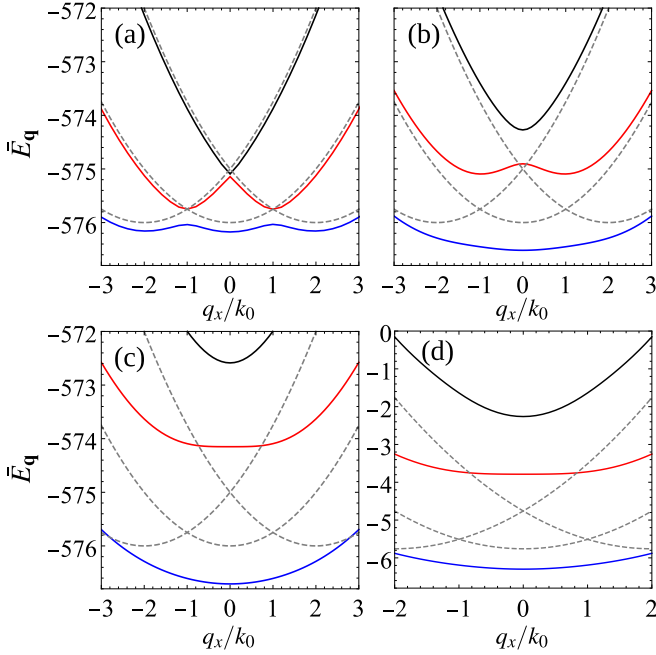


FIG. 1. Energy bands of two-body bound states with symmetric interactions  $a_{\uparrow\uparrow} = a_{\downarrow\downarrow} = a_{\uparrow\downarrow} = a$ . The three parabolic dashed lines in each figure are energy bands at zero Raman strength as a reference, where the three spin channels are decoupled. The dimensionless energy  $\bar{E}_q$  is defined as  $(E_q - 2E_{\min})/(2E_r)$ . (a) Energy bands at  $\Omega = 0.4E_r$  and  $1/(k_0a) = 24$ , where the lowest band has three minima. Formation of these new bands is due to couplings between spin channels. (b) Energy bands at  $\Omega = 2E_r$  and  $1/(k_0a) = 24$ , where the lowest band has only one minimum. (c) Energy bands at  $\Omega = 4E_r$  and  $1/(k_0a) = 24$ , where two minima of the middle band are merged. (d) Energy bands at  $\Omega = 4E_r$  and  $1/(k_0a) = 2.4$ , where all the bands are lifted up due to the increase in  $a$ .

cases, the middle band has only one minimum while the bottom band has one or two minima depending on the Raman strength  $\Omega$ . The minimum energies of these two lower bands are almost the same as the case of symmetric interactions with the same  $a_{\uparrow\downarrow}$ .

The bound-state wave functions can also be solved [30]. In the case with asymmetric interactions  $a_{\uparrow\uparrow} \gg a_{\downarrow\downarrow} = a_{\uparrow\downarrow}$ , we find that at the bottom of the top band the bound state is largely made of atom pairs with spin  $\uparrow\uparrow$  when the Raman strength is weak, as shown in Table I. When the Raman strength increases to the resonance point where the bound-state energy equals to

TABLE I. Bound states of the first band in the case of  $a_{\uparrow\uparrow} = 1500a_0$ ,  $a_{\downarrow\downarrow} = a_{\uparrow\downarrow} = 100a_0$ , and  $1/(k_0a_{\downarrow\downarrow}) = 24$ . The first two columns are in units of  $E_r$ . The momentum is in units of  $\hbar\mathbf{k}_0$ .

$\Omega$	$E_{2\mathbf{q}} - 2E_{\min}$	$2\mathbf{q}$	$\sum_{\mathbf{k}}  \phi_{\uparrow\uparrow} ^2$	$\sum_{\mathbf{k}}  \phi_{\downarrow\downarrow} ^2$	$\sum_{\mathbf{k}}  \phi_{\uparrow\downarrow} ^2$
2	-4.682	-2	0.995	0.00003	0.00234
2	-2.695	0	0.987	0.0004	0.0063
6.9	-1.08	-2	0.924	0.00548	0.0354
6.9	-0.811	-1	0.855	0.0186	0.0633
6.9	-0.0123	0	0.373	0.196	0.216
7.09	0	0	0.25	0.25	0.25

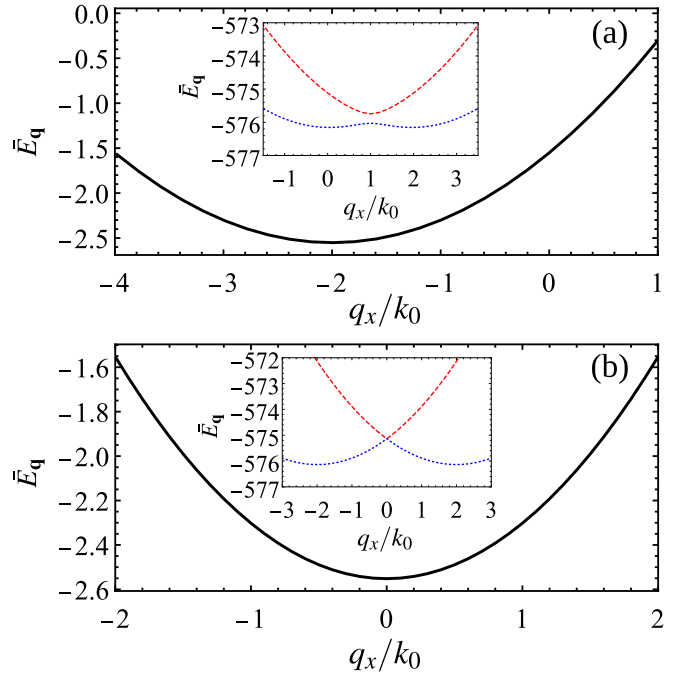


FIG. 2. Bound-state bands with asymmetric interactions at  $\Omega = 0.4E_r$  and  $1/(k_0a_{\downarrow\downarrow}) = 24$ . (a) For  $a_{\downarrow\downarrow} = a_{\uparrow\downarrow} = 100a_0$ , and  $a_{\uparrow\uparrow} = 1500a_0$ , with the Bohr radius  $a_0$ , the top band is shown with the minimum located near  $-2\mathbf{k}_0$  and the bottom two bands are shown in the inset. (b) For  $a_{\downarrow\downarrow} = a_{\uparrow\uparrow} = 100a_0$ , and  $a_{\uparrow\downarrow} = 1500a_0$ , the top band minimum is now located at zero momentum, while the bottom band minima are located near  $\pm 2\mathbf{k}_0$  as shown in the inset.

twice the lowest atom energy, the bound state consists of atom pairs with all the spin configurations.

### III. RESONANCE INDUCED BY SOC

#### A. Resonance condition

At zero Raman strength, the resonance condition is the same as that without SOC, i.e., when the scattering length diverges. At finite Raman strength, the resonance condition changes due to the reconstruction of bound-state bands. In experiments, atoms are often condensed in the two single-particle states with the lowest energy. Since the different spin channels are coupled at finite Raman strength, the resonance occurs whenever the bound-state energy satisfies  $E_{\pm 2\mathbf{q}_0} = 2E_{\min}$  or  $E_0 = 2E_{\min}$ . As a result, multiple resonances can be induced at finite scattering lengths with finite Raman strength.

For symmetric interactions  $a_{\uparrow\uparrow} = a_{\downarrow\downarrow} = a_{\uparrow\downarrow} = a$ , as shown in Figs. 3(a) and 3(b), resonance conditions  $E_{2\mathbf{q}_0} = 2E_{\min}$  and  $E_0 = 2E_{\min}$  are satisfied in the top band at two different scattering lengths for  $\Omega < 4E_r$ . There are in total three different resonances that one can induce by tuning Raman strength  $\Omega$  for each band, but due to symmetry  $E_{2\mathbf{q}_0} = E_{-2\mathbf{q}_0}$  they are located at only two different scattering lengths. When  $\Omega > 4E_r$ , there is only one induced resonance for each band as  $\mathbf{q}_0 = 0$ .

With asymmetric interactions  $a_{\uparrow\uparrow} \gg a_{\downarrow\downarrow} = a_{\uparrow\downarrow}$ , for fixed  $a_{\downarrow\downarrow}$  and  $a_{\uparrow\downarrow}$ , the bound-state energy displays different behavior as a function of  $1/(k_0a_{\uparrow\uparrow})$  in different bands. When  $a_{\uparrow\uparrow}$

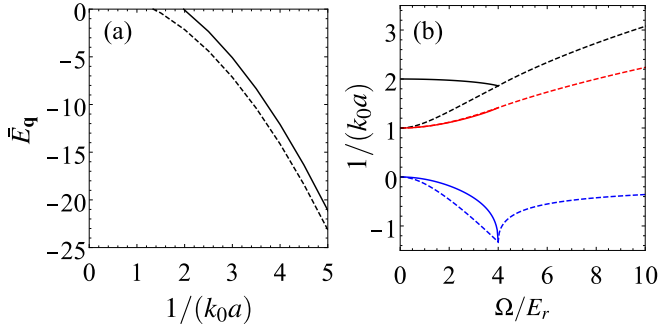


FIG. 3. Induced resonance with symmetric interactions. (a) Bound-state energy in the top band as a function of scattering length  $a$ , where  $\Omega = 2E_r$ . The solid and dashed lines are dimensionless bound-state energy  $\bar{E}_q = (E_q - 2E_{\min})/(2E_r)$  at  $\mathbf{q} = 2\mathbf{q}_0$  and zero, respectively. (b) Scattering length  $a$  vs Raman strength  $\Omega$  at resonances. The solid and dashed lines are for COMM  $2\hbar\mathbf{q}_0$  and zero, respectively. The resonances in the middle band (red lines) occur almost simultaneously for  $\Omega < 4E_r$ , and the red dashed line is simply described by  $\sqrt{-E_{\min}/E_r}$ .

increases, only the top bound-state band can reach the lowest scattering energy  $2E_{\min}$ . The other two bands are insensitive to the change in  $a_{\uparrow\uparrow}$  as shown in Fig. 2(a). When  $\Omega < 4E_r$ , as shown in Fig. 4, there are three induced resonances with COMM  $0, \pm 2\hbar\mathbf{q}_0$ . When  $\Omega > 4E_r$ , there is only one induced resonance.

### B. $T$ matrix and Bethe-Salpeter equation

With finite Raman strength, the effective interactions between atoms are no longer described by the bare coupling constants, but given by the  $T$  matrix which satisfies the Bethe-Salpeter equation, as shown in Fig. 5:

$$\begin{aligned} \mathbf{T}_{\rho_1\rho'_1}^{\rho_2\rho'_2}(q; p \rightarrow k) &= \mathbf{G}_{\rho_1\rho'_1}^{\rho_2\rho'_2} + \sum_{\sigma\sigma'} i \int d^4k' \mathbf{G}_{\rho_1\rho'_1}^{\sigma\sigma'} \\ &\times \mathbf{G}_{\sigma\sigma'}^0(q+k') \mathbf{G}_{\sigma'\sigma'}^0(q-k') \mathbf{T}_{\sigma\sigma'}^{\rho_2\rho'_2}(q; k' \rightarrow k), \end{aligned} \quad (11)$$

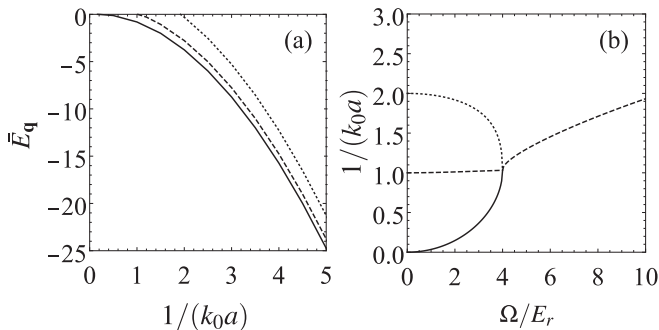


FIG. 4. Induced resonance with asymmetric interactions  $a_{\uparrow\uparrow} \gg a_{\downarrow\downarrow} = a_{\uparrow\downarrow}$  and  $1/(k_0 a_{\uparrow\downarrow}) = 24$ . (a) Bound-state energy in the top band as a function of scattering length  $a_{\uparrow\uparrow}$ , where  $\Omega = 2E_r$ . The solid, dashed, and dotted lines are dimensionless bound-state energy  $\bar{E}_q = (E_q - 2E_{\min})/(2E_r)$  at  $\mathbf{q} = -2\mathbf{q}_0, 0, 2\mathbf{q}_0$ , respectively. (b) Scattering length  $a$  vs Raman strength  $\Omega$  at resonances in the top band. The solid, dashed, and dotted lines are for COMM  $-2\hbar\mathbf{q}_0, 0$ , and  $2\hbar\mathbf{q}_0$ , respectively.

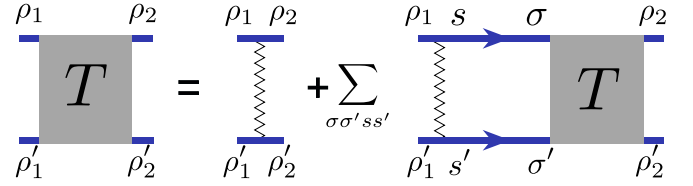


FIG. 5. The diagrams of the Bethe-Salpeter equation.

where  $\rho\rho', \sigma\sigma', ss' \in \{\uparrow\uparrow, \downarrow\downarrow, \uparrow\downarrow, \downarrow\uparrow\}$ ;  $q$  is the center-of-mass four-momentum;  $p, k$ , and  $k'$  are the relative four-momenta with  $k^0 = E$ ; and  $\mathbf{G}$  is the coupling matrix. The Green's-function matrix  $G^0(\mathbf{k}, E)$  is given by

$$G^0(\mathbf{k}, E) = \left[ E - \epsilon_k - \frac{\Omega}{2} \sigma_x - \left( \frac{\hbar^2 k_0}{m} k_x + \frac{\delta}{2} \right) \sigma_z \right]^{-1}. \quad (12)$$

As indicated in Eq. (11),  $\mathbf{T}$  is independent of  $k'$ . Defining the pair susceptibility function  $\chi$ ,

$$\chi_{ss'}^{\rho\rho'}(q) = i \int d^4k' G_{\rho s}^0(q+k') G_{\rho' s'}^0(q-k'), \quad (13)$$

we obtain

$$\mathbf{T} = (\mathbf{I} - \mathbf{G}\chi)^{-1}\mathbf{G}. \quad (14)$$

The coupling matrix can be separated according to statistics,  $\mathbf{G} = \mathbf{G}_{\text{Bose}} + \mathbf{G}_{\text{Fermi}}$ , where

$$\mathbf{G}_{\text{Bose}} = \begin{pmatrix} g_{\uparrow\uparrow} & 0 & 0 & 0 \\ 0 & g_{\downarrow\downarrow} & 0 & 0 \\ 0 & 0 & g_{\uparrow\downarrow}/2 & g_{\uparrow\downarrow}/2 \\ 0 & 0 & g_{\uparrow\downarrow}/2 & g_{\uparrow\downarrow}/2 \end{pmatrix} \quad (15)$$

and

$$\mathbf{G}_{\text{Fermi}} = \begin{pmatrix} 0 & 0 & 0 & 0 \\ 0 & 0 & 0 & 0 \\ 0 & 0 & g_{\uparrow\downarrow}/2 & -g_{\uparrow\downarrow}/2 \\ 0 & 0 & -g_{\uparrow\downarrow}/2 & g_{\uparrow\downarrow}/2 \end{pmatrix}. \quad (16)$$

$T$  matrices for bosons and fermions are decoupled. For fermions, it is reduced to a scalar:

$$\mathbf{T}_f^{-1} = -\frac{m}{4\pi\hbar^2} \left( A_3 - 2C_3 - \frac{1}{a_{\uparrow\downarrow}} \right). \quad (17)$$

For bosons, it can be reduced to a  $3 \times 3$  matrix based on Bose statistics,  $(\mathbf{T}_b)_{\sigma\sigma'}^{\rho\rho'} = \frac{1}{\sqrt{2}}(\mathbf{T}_{\sigma\sigma'}^{\rho\rho'} + \mathbf{T}_{\sigma'\sigma}^{\rho\rho'})$ , and we obtain

$$\mathbf{T}_b^{-1} = \frac{m}{4\pi\hbar^2} (\mathbf{G}'^{-1} - \chi'), \quad (18)$$

where the modified susceptibility is given by

$$\chi' = \begin{pmatrix} A_1 & C_3 & \sqrt{2}C_1 \\ C_3 & A_2 & \sqrt{2}C_2 \\ \sqrt{2}C_1 & \sqrt{2}C_2 & A_3 \end{pmatrix}, \quad (19)$$

with the expressions of  $A_i$  and  $C_j$  given by Eq. (8), and the coupling matrix of bosons in this representation is given by

$$\mathbf{G}' = \begin{pmatrix} a_{\uparrow\uparrow} & 0 & 0 \\ 0 & a_{\downarrow\downarrow} & 0 \\ 0 & 0 & a_{\uparrow\downarrow} \end{pmatrix}. \quad (20)$$

Unsurprisingly the poles of the  $T$  matrix at energy below  $2E_{\min}$  agrees with the bound-state bands as given in Eq. (7). In the absence of SOC, the  $T$  matrix is reduced to bare coupling constants. In the presence of SOC, due to the finite Raman coupling, the effective interaction is no longer given by the bare coupling constants, and the resonance positions are no longer at  $1/a_{\rho\rho'} = 0$ .

### C. Effective interactions near resonance

With symmetric interactions  $a_{\uparrow\uparrow} = a_{\down\down} = a_{\up\down} = a$ , the coupling matrix  $\mathbf{G}'$  is proportional to the identity matrix and Eq. (18) can be rewritten as

$$\mathbf{T}_b^{-1} = \frac{m}{4\pi\hbar^2} \left( \frac{1}{a} \mathbf{I} - \chi' \right), \quad (21)$$

where  $\mathbf{I}$  is the identity matrix. From Eq. (21), the  $T$  matrix can be solved explicitly:

$$\mathbf{T}_b^{-1} = \frac{m}{4\pi\hbar^2} \mathbf{U} \left( \frac{1}{a} \mathbf{I} - \lambda \right) \mathbf{U}^{-1}, \quad (22)$$

where  $\lambda$  and  $\mathbf{U}$  are eigenvalue and unitary transformation matrices of  $\chi'$ ,  $\chi' = \mathbf{U}\lambda\mathbf{U}^{-1}$ ,  $\lambda_{ij} = \delta_{ij}(1/a_{\text{res}}^i)$ , and  $1/a_{\text{res}}^i$  is the  $i$ th eigenvalue of  $\chi'$ . A resonance occurs whenever the scattering length  $a$  is near  $a_{\text{res}}^i$ . The effective interactions near a resonance  $a = a_{\text{res}}^i$  can be approximated by

$$(\mathbf{T}_b)_l^m \approx \frac{4\pi\hbar^2 a_{\text{res}}^i a}{m(a_{\text{res}}^i - a)} \mathbf{U}_l^i \mathbf{U}_m^i, \quad (23)$$

where  $l, m$ , and  $i$  refer to the scattering channels  $\uparrow\uparrow$ ,  $\down\down$ , and  $\up\down$ .

With asymmetric interactions  $a_{\uparrow\uparrow} \gg a_{\down\down} \approx a_{\up\down}$ , we obtain each matrix element of  $\mathbf{T}_b$  in the leading order of  $a_{\up\down}$  as given by

$$\begin{aligned} (\mathbf{T}_b)_{\uparrow\uparrow}^{\uparrow\uparrow} &= \frac{4\pi\hbar^2}{m} \left( \frac{1}{a_{\uparrow\uparrow}} - \chi'_{\uparrow\uparrow} \right)^{-1}, \\ (\mathbf{T}_b)_l^l &= \frac{4\pi\hbar^2}{m} a_l, \\ (\mathbf{T}_b)_l^{\uparrow\uparrow} &= \mathbf{T}_{\uparrow\uparrow}^{\uparrow\uparrow} \chi'_{\uparrow\uparrow}^l a_l, \\ (\mathbf{T}_b)_{\down\down}^{\down\down} &= \mathbf{T}_{\uparrow\uparrow}^{\uparrow\uparrow} \left[ \chi'_{\uparrow\uparrow}^{\down\down} \left( \frac{1}{a_{\uparrow\uparrow}} - \chi'_{\uparrow\uparrow} \right) + \chi'_{\uparrow\uparrow}^{\down\down} \chi'_{\uparrow\uparrow}^{\down\down} \right] a_{\down\down} a_{\up\down}, \end{aligned} \quad (24)$$

where  $l$  refers to either the scattering channel  $\down\down$  or  $\up\down$ . To the leading order of  $a_{\up\down}$ , the dominant interaction near resonance is in the  $\uparrow\uparrow$  channel,  $(\mathbf{T}_b)_{\uparrow\uparrow}^{\uparrow\uparrow} \approx \frac{4\pi\hbar^2}{m} \left( \frac{1}{a_{\uparrow\uparrow}} - A_1 \right)^{-1}$ , and the resonance occurs at  $a_{\uparrow\uparrow} = A_1^{-1}$  where  $A_1 = \chi'_{\uparrow\uparrow}$  is given in Eq. (8).

## IV. DISCUSSION AND CONCLUSION

In experiments,  $^{87}\text{Rb}$  atom gas with Raman-induced SOC is a common platform for studying spin-orbit coupled bosons [31], with a pair of Raman laser beams usually coupling two hyperfine states,  $|\uparrow\rangle = |F=1, m_F=0\rangle$  and  $|\down\rangle = |F=1, m_F=-1\rangle$ . The scattering lengths of different channels are almost equal:  $a_{\uparrow\uparrow} \approx 100.8a_0$  and  $a_{\down\down} = a_{\up\down} \approx$

$100.4a_0$  [5,32]. For counterpropagating Raman laser wavelength 804.1 nm,  $1/(k_0 a_{\up\down}) \approx 24$ . The Raman strength can be tuned up to the order of  $10E_r$ . At  $\Omega = 10E_r$ , we find for symmetric interactions that the resonance position is at  $a = 780a_0$ , much larger than the scattering lengths. It is difficult to observe the induced resonance by adjusting SOC alone. However, the scattering length  $a_{\up\down}$  is tunable by Feshbach resonance [33]. It is possible to observe the induced resonance in the region  $a_{\up\down} \gg a_{\up\down} \approx a_{\down\down}$ . For example, at  $\Omega = 10E_r$ , the resonance position is given by  $a_{\up\down} = 1242a_0$ , for  $1/(k_0 a_{\up\down}) = 24$  shown in Fig. 4(b), available by Feshbach resonance in experiments. When  $\Omega < 4E_r$ , three resonances can be observed instead of one. The resonance induced by SOC has important effects in a Bose gas. Near the resonance, severe particle loss is expected to occur, which may be used as a tool to locate the resonance. Over the resonance, the effective interaction turns to be attractive, and the system is expected to collapse at low temperatures. The effective interaction is strongly modified by SOC near the resonance, and interaction-determined many-body properties are expected to be different from predictions of the simple mean-field theory.

The stripe phase of  $^{87}\text{Rb}$  atoms with SOC is a novel phase which displays both density and superfluid orders, but the density modulation has not been directly imaged so far due to the limited contrast and wavelength of fringes [13,15,34,35]. The induced resonance can be very helpful to solve this problem. Using Feshbach resonance, one can tune up  $a_{\up\down}$  to increase the effective interaction  $\mathbf{T}_{\up\down}^{\up\downarrow}$ , while  $\mathbf{T}_{\down\down}^{\down\down}$  and  $\mathbf{T}_{\up\uparrow}^{\up\uparrow}$  remain almost the same. A compensating detuning laser can be added to offset mean-field shift of energy levels. For example, for atom density about  $10^{14}/\text{cm}^3$  with vertically intersecting Raman lasers of wavelength 804.1 nm, at  $\Omega = 2.6E_r$  and  $\mathbf{T}_{\up\down}^{\up\downarrow} = 5 \times \frac{4\pi\hbar^2}{m} a_{\down\down}$ , following the results from Refs. [34,35], the maximum contrast of fringes in the stripe phase is 0.533 and the period of the stripe is 672 nm, which is observable with current high-resolution-imaging techniques for ultracold atoms [36–40]. Due to the resonance, the critical Raman coupling at the transition from the stripe phase to the plane-wave phase increases significantly to  $\Omega_c = 2.76E_r$  from  $\Omega_c = 0.19E_r$ . The interval length of detuning energy in the stripe phase at  $\Omega = 0E_r$  is also increased to  $1.75E_r$  from  $0.002E_r$ . These results are also helpful to image the stripe structure in experiments.

In summary, we study bound-state bands and resonances in a Bose gas with SOC. We find that finite Raman strength generates coupling among different scattering channels, leading to the reconstruction of bound-state bands. The resonance positions are also shifted due to finite Raman coupling strength, and the effective interactions near these resonances are obtained. We predict that by tuning the scattering length in one intraspecies channel the resonance induced by SOC can be observed in  $^{87}\text{Rb}$  systems, which is helpful to image the density modulation in the stripe phase.

## ACKNOWLEDGMENTS

We would like to thank X.-J. Zhou, Z.-Q. Yu, P. Zhang, and T.-L. Ho for helpful discussions. This work is supported by the National Basic Research Program of China (Grant No. 2016YFA0301501).

- [1] V. Galitski and I. B. Spielman, Spin-orbit coupling in quantum gases, *Nature (London)* **494**, 49 (2013).
- [2] N. Goldman, G. Juzeliūnas, P. Öhberg, and I. B. Spielman, Light-induced gauge fields for ultracold atoms, *Rep. Prog. Phys.* **77**, 126401 (2014).
- [3] H. Zhai, Degenerate quantum gases with spin-orbit coupling: A review, *Rep. Prog. Phys.* **78**, 026001 (2015).
- [4] S.-L. Zhang and Q. Zhou, Manipulating novel quantum phenomena using synthetic gauge fields, *J. Phys. B* **50**, 222001 (2017).
- [5] Y.-J. Lin, K. Jimenez-Garcia, and I. B. Spielman, Spin-orbit-coupled Bose-Einstein condensates, *Nature (London)* **471**, 83 (2011).
- [6] P. Wang, Z.-Q. Yu, Z. Fu, J. Miao, L. Huang, S. Chai, H. Zhai, and J. Zhang, Spin-Orbit Coupled Degenerate Fermi Gases, *Phys. Rev. Lett.* **109**, 095301 (2012).
- [7] L. W. Cheuk, A. T. Sommer, Z. Hadzibabic, T. Yefsah, W. S. Bakr, and M. W. Zwierlein, Spin-Injection Spectroscopy of a Spin-Orbit Coupled Fermi Gas, *Phys. Rev. Lett.* **109**, 095302 (2012).
- [8] L. Huang, Z. Meng, P. Wang, P. Peng, S.-L. Zhang, L. Chen, D. Li, Q. Zhou, and J. Zhang, Experimental realization of two-dimensional synthetic spin-orbit coupling in ultracold Fermi gases, *Nat. Phys.* **12**, 540 (2016).
- [9] Z. Wu, L. Zhang, W. Sun, X.-T. Xu, B.-Z. Wang, S.-C. Ji, Y. Deng, S. Chen, X.-J. Liu, and J.-W. Pan, Realization of two-dimensional spin-orbit coupling for Bose-Einstein condensates, *Science* **354**, 83 (2016).
- [10] S.-C. Ji, J.-Y. Zhang, L. Zhang, Z.-D. Du, W. Zheng, Y.-J. Deng, H. Zhai, S. Chen, and J.-W. Pan, Experimental determination of the finite-temperature phase diagram of a spin-orbit coupled Bose gas, *Nat. Phys.* **10**, 314 (2014).
- [11] Y. Li, L. P. Pitaevskii, and S. Stringari, Quantum Tricriticality and Phase Transitions in Spin-Orbit Coupled Bose-Einstein Condensates, *Phys. Rev. Lett.* **108**, 225301 (2012).
- [12] S.-C. Ji, L. Zhang, X.-T. Xu, Z. Wu, Y. Deng, S. Chen, and J.-W. Pan, Softening of Roton and Phonon Modes in a Bose-Einstein Condensate with Spin-Orbit Coupling, *Phys. Rev. Lett.* **114**, 105301 (2015).
- [13] J.-R. Li, J. Lee, W. Huang, S. Burchesky, B. Shteynas, F. Ç. Top, A. O. Jamison, and W. Ketterle, A stripe phase with supersolid properties in spin-orbit-coupled Bose-Einstein condensates, *Nature (London)* **543**, 91 (2017).
- [14] T. M. Bersano, J. Hou, S. Mossman, V. Gokhroo, X.-W. Luo, K. Sun, C. Zhang, and P. Engels, Experimental realization of a long-lived striped Bose-Einstein condensate induced by momentum-space hopping, *Phys. Rev. A* **99**, 051602(R) (2019).
- [15] A. Putra, F. Salces-Cárcoba, Y. Yue, S. Sugawa, and I. B. Spielman, Spatial Coherence of Spin-Orbit-Coupled Bose Gases, *Phys. Rev. Lett.* **124**, 053605 (2020).
- [16] H. Hu, L. Jiang, X.-J. Liu, and H. Pu, Probing Anisotropic Superfluidity in Atomic Fermi Gases With Rashba Spin-Orbit Coupling, *Phys. Rev. Lett.* **107**, 195304 (2011).
- [17] K. Seo, L. Han, and C. A. R. Sá de Melo, Emergence of Majorana and Dirac Particles in Ultracold Fermions Via Tunable Interactions, Spin-Orbit Effects, and Zeeman Fields, *Phys. Rev. Lett.* **109**, 105303 (2012).
- [18] F. Wu, G.-C. Guo, W. Zhang, and W. Yi, Unconventional Superfluid in a Two-Dimensional Fermi Gas with Anisotropic Spin-Orbit Coupling and Zeeman Fields, *Phys. Rev. Lett.* **110**, 110401 (2013).
- [19] Z.-Q. Yu and H. Zhai, Spin-Orbit Coupled Fermi Gases Across a Feshbach Resonance, *Phys. Rev. Lett.* **107**, 195305 (2011).
- [20] J. P. Vyasanakere, S. Zhang, and V. B. Shenoy, BCS-BEC crossover induced by a synthetic non-Abelian gauge field, *Phys. Rev. B* **84**, 014512 (2011).
- [21] R. Li and L. Yin, Pair condensation in a dilute Bose gas with Rashba spin-orbit coupling, *New J. Phys.* **16**, 053013 (2014).
- [22] D. Luo and L. Yin, BCS-pairing state of a dilute Bose gas with spin-orbit coupling, *Phys. Rev. A* **96**, 013609 (2017).
- [23] R. A. Williams, L. J. LeBlanc, K. Jiménez-García, M. C. Beeler, A. R. Perry, W. D. Phillips, and I. B. Spielman, Synthetic partial waves in ultracold atomic collisions, *Science* **335**, 314 (2012).
- [24] J. P. Vyasanakere and V. B. Shenoy, Bound states of two spin- $\frac{1}{2}$  fermions in a synthetic non-Abelian gauge field, *Phys. Rev. B* **83**, 094515 (2011).
- [25] L. Zhang, Y. Deng, and P. Zhang, Scattering and effective interactions of ultracold atoms with spin-orbit coupling, *Phys. Rev. A* **87**, 053626 (2013).
- [26] R. A. Williams, M. C. Beeler, L. J. LeBlanc, K. Jiménez-García, and I. B. Spielman, Raman-Induced Interactions in a Single-Component Fermi Gas Near an *s*-Wave Feshbach Resonance, *Phys. Rev. Lett.* **111**, 095301 (2013).
- [27] S.-J. Wang and C. H. Greene, Spin-orbit-induced resonances and threshold anomalies in a reduced-dimension Fermi gas, *Phys. Rev. A* **94**, 053635 (2016).
- [28] Q. Gu and L. Yin, Spin-orbit-coupling-induced resonance in an ultracold Bose gas, *Phys. Rev. A* **98**, 013617 (2018).
- [29] Z. Lan and P. Öhberg, Raman-dressed spin-1 spin-orbit-coupled quantum gas, *Phys. Rev. A* **89**, 023630 (2014).
- [30] One can obtain the wave function from  $\Phi_{\mathbf{kq}} = M_{\mathbf{kq}}^{-1} \Gamma_i$ , where  $\Gamma_i$  is the *i*th eigenvector of  $(\mathbf{G} \frac{1}{V} \sum_{\mathbf{k}} M_{\mathbf{kq}}^{-1} - \mathbf{I})$  with eigenvalue  $\lambda_i(E_{2q}) = 0$ .
- [31] R. Wei and E. J. Mueller, Magnetic-field dependence of Raman coupling in alkali-metal atoms, *Phys. Rev. A* **87**, 042514 (2013).
- [32] E. G. M. van Kempen, S. J. J. M. F. Kokkelmans, D. J. Heinzen, and B. J. Verhaar, Interisotope Determination of Ultracold Rubidium Interactions from Three High-Precision Experiments, *Phys. Rev. Lett.* **88**, 093201 (2002).
- [33] A. Marte, T. Volz, J. Schuster, S. Dürr, G. Rempe, E. G. M. van Kempen, and B. J. Verhaar, Feshbach Resonances in Rubidium 87: Precision Measurement and Analysis, *Phys. Rev. Lett.* **89**, 283202 (2002).
- [34] G. I. Martone, Y. Li, and S. Stringari, Approach for making visible and stable stripes in a spin-orbit-coupled Bose-Einstein superfluid, *Phys. Rev. A* **90**, 041604(R) (2014).
- [35] G. I. Martone, Visibility and stability of superstripes in a spin-orbit-coupled Bose-Einstein condensate, *Eur. Phys. J.: Spec. Top.* **224**, 553 (2015).
- [36] W. S. Bakr, J. I. Gillen, A. Peng, S. Fölling, and M. Greiner, A quantum gas microscope for detecting single atoms in a Hubbard-regime optical lattice, *Nature (London)* **462**, 74 (2009).

- [37] M. Stecker, H. Schefzyk, J. Fortágh, and A. Günther, A high resolution ion microscope for cold atoms, [New J. Phys.](#) **19**, 043020 (2017).
- [38] S. Häusler, S. Nakajima, M. Lebrat, D. Husmann, S. Krinner, T. Esslinger, and J.-P. Brantut, Scanning Gate Microscope for Cold Atomic Gases, [Phys. Rev. Lett.](#) **119**, 030403 (2017).
- [39] M. McDonald, J. Trisnadi, K.-X. Yao, and C. Chin, Superresolution Microscopy of Cold Atoms in An Optical Lattice, [Phys. Rev. X](#) **9**, 021001 (2019).
- [40] S. Subhankar, Y. Wang, T.-C. Tsui, S. L. Rolston, and J. V. Porto, Nanoscale Atomic Density Microscopy, [Phys. Rev. X](#) **9**, 021002 (2019).